HAL
open science

Signatures of the midnight open-closed magnetic field line boundary during balanced dayside and nightside reconnection

M. L. Parkinson, P. L. Dyson, M. Pinnock, J. C. Devlin, M. R. Hairston, E. Yizengaw, P. J. Wilkinson

To cite this version:

M. L. Parkinson, P. L. Dyson, M. Pinnock, J. C. Devlin, M. R. Hairston, et al.. Signatures of the midnight open-closed magnetic field line boundary during balanced dayside and nightside reconnection. Annales Geophysicae, 2002, 20 (10), pp.1617-1630. hal-00317180

HAL Id: hal-00317180

https://hal.science/hal-00317180v1

Submitted on 18 Jun 2008

HAL is a multi-disciplinary open access archive for the deposit and dissemination of scientific research documents, whether they are published or not. The documents may come from teaching and research institutions in France or abroad, or from public or private research centers.

L'archive ouverte pluridisciplinaire **HAL**, est destinée au dépôt et à la diffusion de documents scientifiques de niveau recherche, publiés ou non, émanant des établissements d'enseignement et de recherche français ou étrangers, des laboratoires publics ou privés.

Annales Geophysicae (2002) 20: 1617–1630 © European Geosciences Union 2002

Signatures of the midnight open-closed magnetic field line boundary during balanced dayside and nightside reconnection

M. L. Parkinson[1], P. L. Dyson[1], M. Pinnock[2], J. C. Devlin[3], M. R. Hairston[4], E. Yizengaw[1], and P. J. Wilkinson[5]

[1]Department of Physics, La Trobe University, Victoria 3086, Australia
[2]British Antarctic Survey, Natural Environment Research Council, Cambridge CB3 0ET, UK
[3]Department of Electronic Engineering, La Trobe University, Victoria 3086, Australia
[4]William B. Hanson Center for Space Sciences, University of Texas at Dallas, Richardson, Texas, USA
[5]IPS Radio and Space Services, Sydney, New South Wales 1240, Australia

Received: 1 September 2001 – Revised: 29 March 2002 – Accepted: 30 April 2002

Abstract. The geomagnetic conditions were moderately disturbed (K_p=2) during magnetic midnight on 10 December 1999, when the Tasman International Geospace Environment Radar (TIGER), a Southern Hemisphere HF SuperDARN radar, observed a persistent, sharp latitudinal decrease (∼90 km) in spectral width near −69° Λ. The line-of-sight Doppler velocity also rapidly declined across this spectral width boundary (SWB). The region poleward of the SWB was characterized by high spectral widths (>200 m/s), and the start of bursty equatorward and eastward flows (>500 m/s), which rapidly expanded equatorward. The relationships between familiar ionospheric and magnetospheric regions were inferred by comparing TIGER data with spectrograms calculated from precipitating particles measured on board the Defence Meteorology Satellite Program (DMSP) F14 satellite. The high spectral width scatter is often observed, and on this evening it was associated with irregularities forming on the open (but soon to be reconnected) field lines threading the polar cap ionosphere to the southern tail lobe. The region equatorward of the SWB was characterized by very low spectral widths (<50 m/s) and generally slower, more zonal flows (<300 m/s). This kind of scatter is more transient, and was associated with irregularities residing on the closed field lines threading the discrete and diffuse auroral oval to the plasma sheet boundary layer (PSBL) and central plasma sheet (CPS). Hence, the SWB was a reasonable proxy for the open-closed field line boundary, and the equatorward limit of the region, with low spectral width, was probably aligned with the poleward wall of the main ionospheric trough. The SWB was observed to contract poleward and expand equatorward on time scales of ∼10 min, much as would be expected during balanced dayside and nightside reconnection. Total electron content (TEC) measurements made at Macquarie Island (−65° Λ) and Hobart (−54° Λ), and the ionograms recorded at the same stations, as well as at Bundoora (−49° Λ), also helped to validate the interpretation.

Correspondence to: M. L. Parkinson
(m.parkinson@latrobe.edu.au)

Key words. Ionosphere (auroral ionosphere; electric fields and currents; ionosphere-magnetosphere interactions)

1 Introduction

The Super Dual Auroral Radar Network (SuperDARN) consists of HF backscatter radars imaging high-latitude ionospheric convection on a global scale (Greenwald et al., 1985, 1995). Monitoring the ionospheric footprint of magnetospheric boundaries is a potentially useful space-weather application of SuperDARN. For example, the equatorward edge of the region of large Doppler spectral width associated with the footprint of the cusp in the dayside ionosphere probably corresponds to the open-closed field line boundary (OCB) when the interplanetary magnetic field (IMF) is southward (e.g. Baker et al., 1995; Milan et al., 1998; and Moen et al., 2001). This dayside signature expands rapidly equatorward and contracts poleward in unison with decreases and increases in the IMF B_z component, respectively (Pinnock et al., 1993). R. A. Greenwald (Private Communication) used the dawn and dusk convection reversal boundary (CRB) identified in SuperDARN derived maps of convection potential as a proxy for the OCB.

A sharp nightside transition between regions of scatter with large (>200 m/s) and small (<50 m/s) Doppler spectral widths is sometimes observed poleward of 69° S during geomagnetic quiet conditions. The magnetospheric mapping of this spectral width boundary (SWB) is more contentious. Lewis et al. (1997, 1998) studied substorm signatures in SuperDARN data and suggested that the nightside SWB mapped to the boundary between the boundary plasma sheet (BPS) (discrete aurora) and the central plasma sheet (CPS) (diffuse aurora). Dudeney et al. (1998) studied an example of a gradual nightside SWB in Halley HF radar data, and compared its location with Polar spacecraft measurements made during a favourable transit. They also associated the SWB with the BPS/CPS boundary. The Polar

electrostatic wave data also suggested an association between enhanced spectral width and power in the Pc1–2 band.

However, when Yeoman et al. (1999) studied substorm signatures in HF radar data and coincident Defence Meteorological Satellite Program (DMSP) precipitation measurements, they found no systematic agreement between the CPS/BPS boundary and a boundary in the spectral widths. More recently, Lester et al. (2001) reported an example in which the pre-midnight SWB was collocated with the poleward edge of the 630.0 nm auroral emission, which may also locate the OCB (Blanchard et al., 1995). In yet another case study, Woodfield et al. (2002) only found partial agreement between the post-midnight SWB and the poleward edge of 630.0 nm optical aurora emission. Rather, they found an association between large spectral widths and elevated electron temperatures, and noted the need to investigate the relationship between the SWB and the OCB versus magnetic local time (MLT).

Blanchard et al. (1997) further investigated the accuracy of using the poleward edge of the 630.0 nm auroral emission to identify the OCB. After excluding cases with gross errors, presumably due to longitudinal structure during auroral substorms, they gave $\pm 1.5°$ as a conservative estimate for the error in the technique. Most of their data was in the pre-midnight sector, and a rough proxy for the OCB, such as the poleward edge of the 630.0 nm auroral emission, has limited use for validating the identity of the radar SWB. Identification of the OCB using spacecraft data has potentially greater accuracy for this purpose.

Clearly, different instrumental techniques rely on different physical processes to infer the location of the OCB. The different proxies may not always be in close agreement, depending on the prevailing geophysical conditions. Indeed, the character of the proxies can even change in observations made with the same instrument (e.g. the radar SWB can be gradual, sharp, or bifurcated). Many more multi-instrument case studies must be analyzed to help resolve these issues, including to what extent the nightside SWB represents the OCB. The results of these studies will also facilitate a deeper understanding of statistical plots of SuperDARN spectral widths (e.g. André et al., 2002).

The SuperDARN radar network cannot image a complete picture of the auroral oval beyond dusk because, even for moderate levels of geomagnetic activity, the oval expands equatorward of the preferred range windows for backscatter constrained by the radar location and available propagation channels. The Tasman International Geospace Environment Radar (TIGER) (Dyson and Devlin, 2000) is a SuperDARN radar located on Bruny Island (43.4° S, 147.2° E geographic), Tasmania. TIGER's default range window, 180 to 3555 km, extends from magnetic latitude (Λ) 57° S to 88° S, which is $\sim 5° \Lambda$ equatorward of the high-latitude ionosphere imaged by most of the other radars. TIGER can provide a more complete picture of geomagnetically quiet auroral and sub-auroral processes in the midnight sector. Hence, we believe that TIGER observations will help to clarify the interpretation of nightside Doppler velocity signatures, including the SWB, and other substorm-related processes.

In this paper, we focus on a 3 h set of high-time resolution, 6 s observations made by TIGER during moderately disturbed geomagnetic conditions (K_p=2) on the evening of 10 December 1999. A very clear and persistent SWB in the nightside ionospheric scatter was observed, as well as the signatures of other interesting phenomena, including patches of decametre-scale irregularities advecting across the polar cap. The DMSP F14 spacecraft made a favourable transit through the TIGER field-of-view (FOV) during the study interval, enabling the corresponding magnetospheric regions to be identified. We could also infer the probable locations of low-altitude structures, such as the main ionospheric trough, by consulting ionosonde and total electron content (TEC) measurements made on various days, encompassing a broad range of geomagnetic conditions. These ground-based observations were made at Hobart (HOB) (42.9° S, 147.3° E; $-54° \Lambda$), Macquarie Island (MQI) (54.5° S, 158.9° E; $-65° \Lambda$), and Tidbinbilla (TBL) (35.4° S, 149.0° E; $-46° \Lambda$).

In this paper, we will interpret our multi-instrument data in the context of the following familiar picture of coupled, nightside ionosphere-magnetosphere dynamics:

1. The OCB in the nightside magnetosphere separates open magnetic flux tubes mapping to the tail lobes from the closed field lines of the outer central plasma sheet (CPS) (e.g. Kivelson and Russell, 1995). The northern and southern tail lobes map to the corresponding nightside polar cap. The OCB is coincident with the poleward limit of the discrete auroral oval, which resides on closed field lines mapping to the outer CPS (Vampola, 1971; Evans and Stone, 1972).

2. The plasma sheet boundary layer (PSBL) separates the tail lobes from the CPS, and might be formed by nightside magnetic reconnection during sustained B_z southward conditions. Nightside reconnection is thought to be most vigorous during magnetospheric substorms; hence, the PSBL will be most developed then. The turbulent nightside PSBL is analogous to the dayside low-latitude boundary layer (LLBL), which might be formed by dayside merging. In one "classical" picture, the PSBL maps to the low altitude boundary plasma sheet (BPS), which is also the region of discrete auroral precipitation (e.g. see Winningham et al., 1975). However, this picture has been disputed by Newell et al. (1996), who argued that discrete auroral structures also map to the CPS.

3. The inner edge of the CPS maps to the equatorward limit of the diffuse auroral zone, which also corresponds to the field-aligned poleward wall of the main ionospheric trough, especially during the pre-midnight hours (Rodger et al., 1986; Dudeney and Rodger, 1988). However, the locations of discrete aurora can move

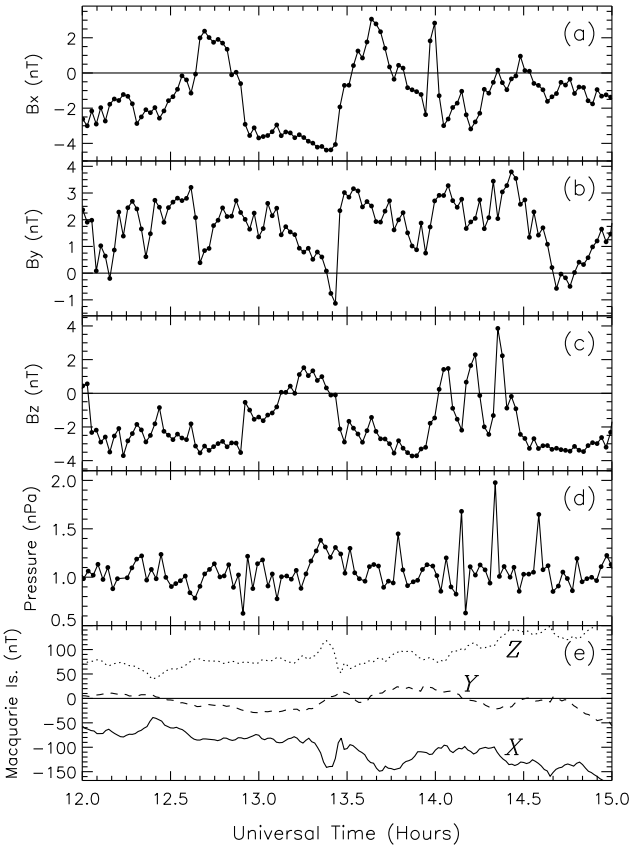

Fig. 1. Wind spacecraft measurements of the IMF **(a)** B_x, **(b)** B_y, and **(c)** B_z components, and **(d)** the solar wind dynamic pressure, all averaged to ∼1.5 min time resolution during 12:00 to 15:00 UT on 10 December 1999. **(e)** Perturbations of the geomagnetic X (solid curve), Y (dashed curve), and Z (dotted curve) components measured at the Macquarie Island (MQI) magnetometer (provided courtesy of the Australian Geological Survey Organisation). The abscissas have tick marks at 5 min intervals of UT.

equatorward during geomagnetic storms and subsequently reform the poleward wall of the trough. The latter is a very sharp feature, often forming in association with boundary blobs convected from the dayside, or created by local auroral precipitation (Tsunoda, 1988).

4. Some authors have associated the ionospheric projection of the plasmapause with the location of the main trough (Rodger and Pinnock, 1982; Smith et al., 1987). However, it is well-known that the outer limits of the plasmasphere may actually consist of a series of ledges, disappearing and reforming in accordance with the history of geomagnetic activity spanning many days (Carpenter and Park, 1973). It takes many hours for ionospheric plasma to diffuse upwards and refill plasmaspheric flux tubes (Web and Essex, 2001). Hence, the association between the trough and plasmapause is a loose one, more likely to be valid during the growth phase of a geomagnetic storm, than the recovery phase.

Of course, the above summary is a simplified picture of some very dynamic processes interacting with each other in many complicated ways. Furthermore, the formation and evolution of the different magnetospheric boundaries are only partly understood for a limited range of geophysical conditions. TIGER is located far enough equatorward to image the low-latitude limit of these dynamic processes. In this paper, we propose a plausible scenario that explains our results, but further statistical work is required before they can be generalised to other events.

2 Observations and interpretation

During 12:00 to 15:00 UT on 10 December 1999, the Wind spacecraft was located above the equatorial plane on the dawn side of the magnetosphere at geocentric solar magnetospheric (GSM) x, y, and z coordinates of ~ -28, -59, and $25\,R_E$, respectively. Figure 1 shows Wind measurements of the interplanetary magnetic field (IMF) components in GSM coordinates (parts a-c), and the solar wind dynamic pressure (part d). Lepping et al. (1995) and Ogilvie et al. (1995) describe the instruments used to make the IMF and solar wind observations, respectively. B_y was primarily positive, fluctuating in the range 1–3 nT, but brief negative excursions in B_y started at 13:23 and 14:40 UT. B_z was primarily negative at about -3 nT, but there were several weak northward excursions at about 13:15, 14:03, 14:13, and 14:21 UT. The dynamic pressure was essentially steady at around 1 nPa, but there were significant (>50%) impulsive increases at 14:09, 14:20, and 14:35 UT. Although not critical to the event interpretation, we note the GSM x location of Wind and the representative solar wind speed of ∼480 km/s imply an ∼6 min delay for the solar wind conditions to affect the noon-sector ionosphere.

Figure 1e shows MQI ($-65°\Lambda$) magnetometer perturbations in the geomagnetic X (north), Y (east), and Z (down) components. These measurements were de-spiked and then de-trended by subtracting a baseline defined by their average diurnal values. The perturbations occurring during 10 December were modest by the standards of the perturbations observed on most nights at this auroral station. However, the X and Y components at MQI did exhibit moderate growth-phase behaviour throughout the study interval, with the signature of a -150 nT pseudo-breakup occurring just beyond 15:00 UT.

Applying the right-hand screw rule to the magnitude and sense of all three components of the magnetometer deflections shown in Fig. 1e suggests the ionospheric Hall current flowed toward the west and poleward, but centred several hundred kilometres poleward of the station. Reinterpreted as F-region drifts, this implies that the plasma convected toward the east and equatorward, as will be shown by analysing TIGER beam-swinging measurements. The magnetometer measurements are also consistent with the discrete auroral oval residing just poleward of MQI during 12:00 to 15:00 UT, as will be confirmed using DMSP F14 measurements.

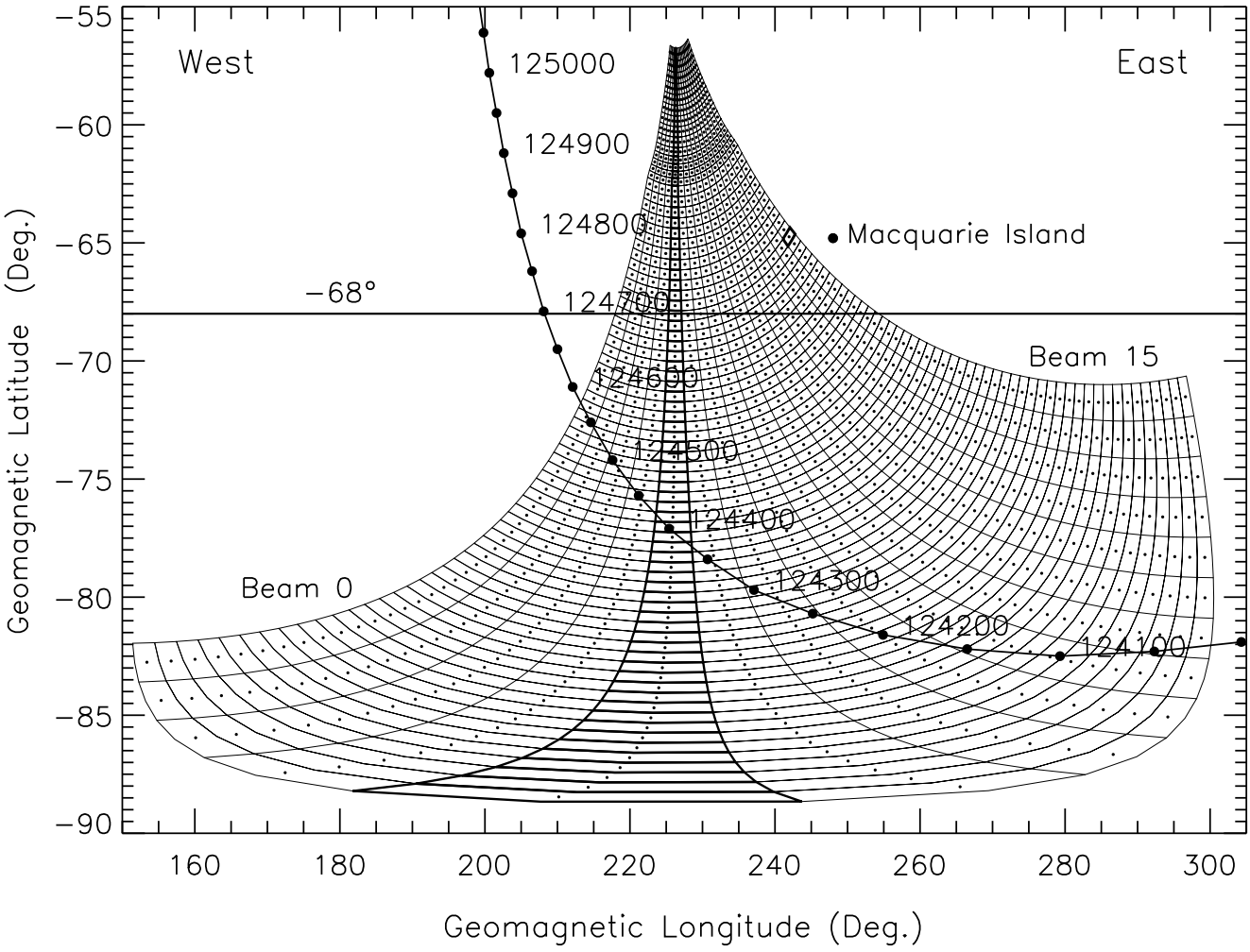

Fig. 2. The track of the DMSP F14 spacecraft through the TIGER field-of-view during 12:40:00 to 12:51:00 UT, 10 December 1999. The satellite track and the 75 range cells sampled on each of the 16 beams of TIGER have been plotted on the same grid of magnetic latitude and longitude. Beam 0 is the western-most beam (left) and beam 15 is the eastern-most beam (right). Beam 4, drawn in bold, points along the 226° E magnetic meridian, but diverges towards the west at higher latitude. Range cell 26 of beam 15 is also drawn in bold because it is the closest observation cell to MQI on the same L-shell.

The K_p index was 2 during 12:00 to 15:00 UT, and only 1+ during the preceding three-hour interval. Overall, the conditions were moderately disturbed. We note that strong substorm signatures are usually observed in nighttime magnetograms recorded at MQI, when B_z is southward for prolonged intervals. The absence of a distinct substorm above MQI during the study interval implies there may have been an ongoing balance between dayside and nightside reconnection until beyond 15:00 UT. The brief B_z northward excursions may have slowed the accumulation of magnetic flux in the magnetotail without triggering a full substorm in this instance.

The preceding interpretation was supported by LAN-L geosynchronous spacecraft measurements of energetic particle injections; when a spacecraft is located in the initial injection region, a dispersionless particle injection indicative of expansion onset will be observed (Henderson et al., 1996). Injections observed by LAN-L 1994–084 at ∼14:46 UT (21:53 MLT) and ∼15:08 UT (22:13 MLT) had the characteristics of pseudo-breakups, and not of full substorm onsets. An injection did not have the characteristic of a full substorm until ∼15:40 UT (22:43 MLT), namely a sustained, enhanced electron flux lasting ∼1 h, which then decayed.

Figure 2 shows that MQI had the same magnetic latitude as range cell 26 (1350 km; bold) of TIGER beam 15. The high time resolution (6 s) beam 4 is also shown in bold. Figure 2 also shows the ionospheric track of the DMSP F14 spacecraft coincident with the TIGER FOV during the study interval. The DMSP spacecraft are in Sun synchronous, near polar orbits, with an altitude of 830 km and a period of 101 min (e.g. Anderson et al., 1997). The magnetic coordinates of the satellite track were calculated using Tsyganenko (1990) magnetic field lines (see Tsyganenko and Stern, 1996, and references therein) passing through the satellite down to an ionospheric footprint at an altitude 110 km. The map-

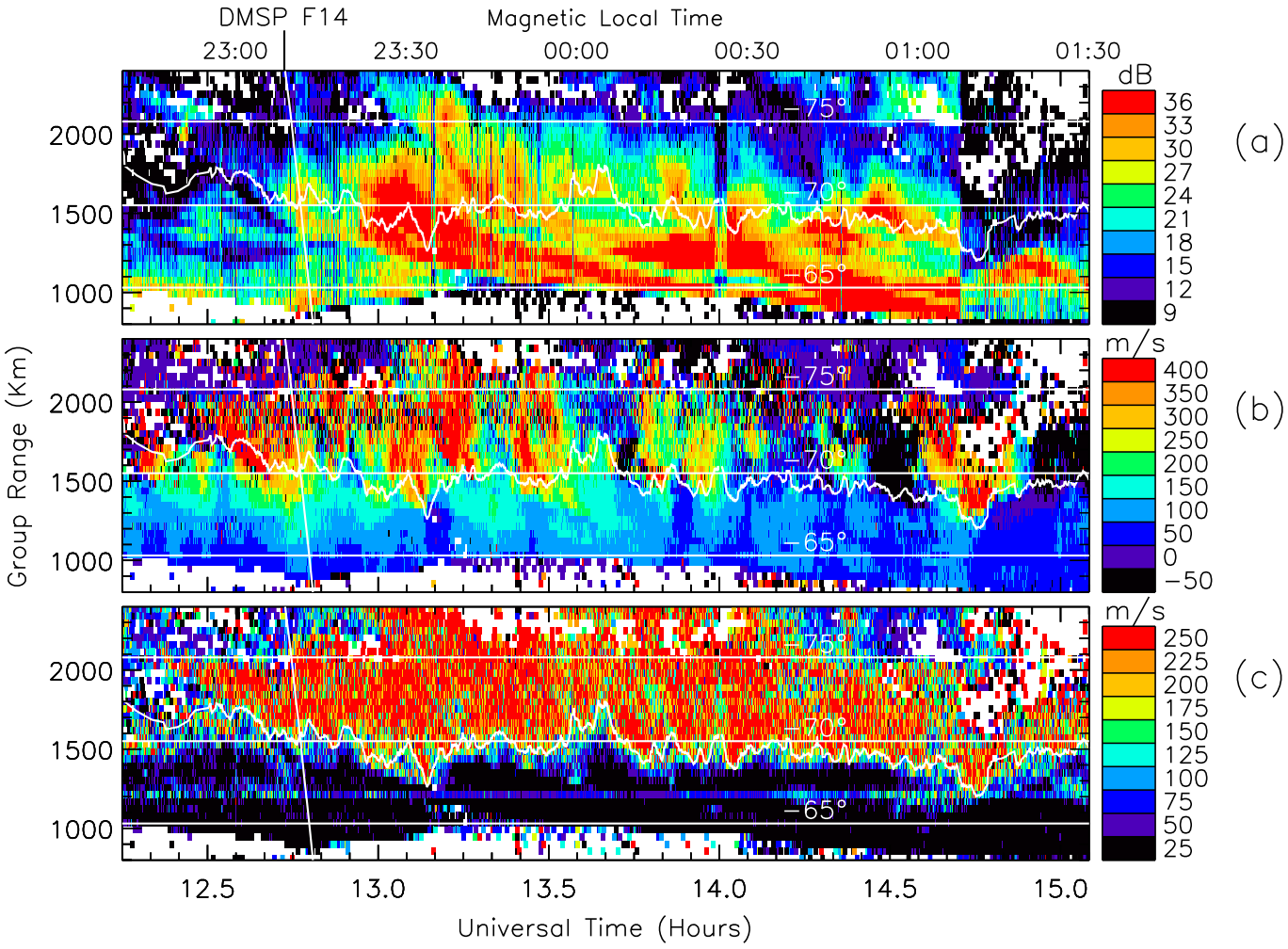

Fig. 3. RTI plots of **(a)** TIGER backscatter power (dB), **(b)** LOS Doppler velocity (m/s), and **(c)** spectral width (m/s) recorded on beam 4 during 12:15 to 15:00 UT, 10 December 1999. The spectral width boundary (SWB) was automatically identified (as explained in the text) and has been superimposed in all panels. The three thin, white horizontal lines in all panels correspond to AACGM latitudes of −65° (MQI), −70°, and −75°. Diagonal white lines starting at 12:45 UT in all three panels represent the transit of the DMSP F14 satellite (cf., Fig. 2). The patchy horizontal line in the data samples at range 1215 km in (c) corresponds to a bad range in the autocorrelation function. The abscissas have tick marks at 5 min intervals of UT, and nominal values of MLT separated by 30 min intervals are included at top.

ping procedures should be accurate to <1°, and thus, can be used to reliably locate the auroral oval with respect to the radar data.

The azimuths and group delays of TIGER observation cells were mapped to altitude adjusted and corrected geomagnetic coordinates (AACGM) (Baker and Wing, 1989), assuming a virtual reflection height of 300 km. This is a standard assumption made in numerous SuperDARN studies, and it seems to work well. The true heights of the backscattering irregularities can be much lower, but there is only a ∼0.1° difference between the magnetic latitude of points located at true heights 110 and 300 km at the range of our SWB observations. Without performing detailed ray-tracing calculations for the actual ionospheric conditions on 10 December, we surmise that the TIGER magnetic latitudes were also accurate to <1°. Hence, we consider $\sim\sqrt{2}°$ to be the maximum conceivable error in a comparison between DMSP and TIGER observations, though probably much less.

Figure 3 shows range-time-intensity (RTI) plots of (a) the backscatter power (dB), (b) LOS Doppler velocity (m/s), and (c) Doppler spectral width (m/s) measured on TIGER beam 4 during 12:15 to 15:00 UT on 10 December 1999. The three parameters were calculated using the standard "FITACF" algorithm (Baker et al., 1995) used to process all SuperDARN autocorrelation measurements. Any echoes FITACF identified as coming from the sea were rejected in this study. As mentioned, beam 4 results are shown because they were recorded with a 6 s time resolution. This was achieved by interleaving them with normal 16-beam scans using 3 s integration times. Thus, each full scan took 96 s to complete. The UT interval shown corresponds to the nominal magnetic midnight interval 22:40 to 01:30 MLT.

Figure 3a shows power colour-coded from black for signal-to-noise ratios (SNRs) ≤9 dB to red for SNRs ≥36 dB.

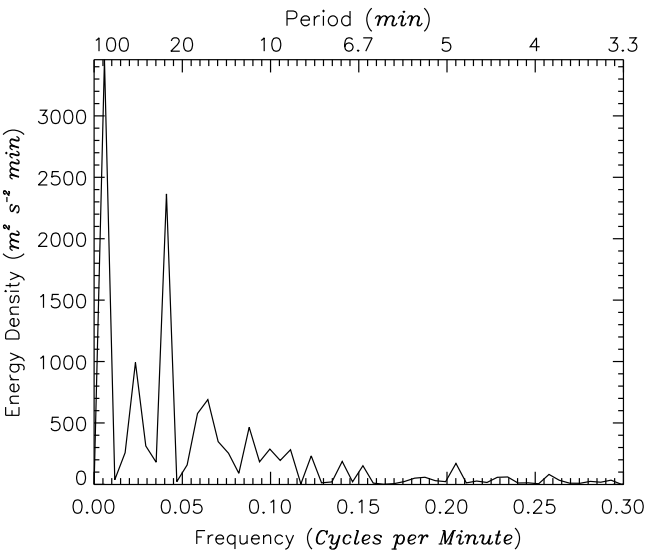

Fig. 4. Power spectrum of LOS Doppler velocities recorded at range cell 36 (1800 km) on TIGER beam 4 during 12:15 to 15:00 UT, 10 December 1999. Isolated Doppler velocity spikes further than 3 standard deviations from the mean were suppressed to remove high-frequency noise from the power spectrum.

The operating frequency for these measurements was typically 11.9 MHz, but the radar control program made numerous automatic changes in frequency of ∼100 kHz to mitigate radio interference, but only with partial success. The step-like decreases in SNR were primarily due to increases in the noise floor, because it is unlikely that small changes in operating frequency would select propagation paths with completely different refraction. Some of the deleterious effects of the longer-lasting interference started at 13:09, 13:59, and 14:42 UT. The record demonstrates the importance of selecting a noise free, fixed frequency to preserve the continuity of many ionospheric measurements.

Figure 3a shows a sequence of patches of enhanced SNR migrating equatorward, initially at speeds of >500 m/s (to be shown), but subsequently decelerating towards the lowest latitudes. The patches generally drifted equatorward and, as will be seen in Fig. 5, eastward. This motion was presumably coincident with the migration of conditions favourable to the production of decametre-scale irregularities with large $\delta n_e/n_e$ (where n_e is the electron density). Some of the patches were detected just beyond $-77°\Lambda$, but they generally had the largest SNRs equatorward of $-72°\Lambda$. Some of the well-defined patches preserved their identity over changes in range >600 km, but this may partly represent the range window imaged by the same F-region propagation mode.

Figure 3a shows the most prominent power enhancement commenced at ∼12:56 UT and $-72°\Lambda$, and can probably be traced all the way to ∼14:42 UT and $-63°\Lambda$ (i.e. Δrange ∼1000 km). However, this main feature may have been first detected as a weak enhancement at ∼12:45 UT and $-77°\Lambda$. Another power enhancement expanded equatorward, just equatorward of the main feature, losing its identity at ∼13:35 UT and $-65°\Lambda$. This feature may have been first detected as a weak enhancement at ∼12:15 UT and $-77°\Lambda$. Another clearly recognisable power enhancement, probably commencing as early as ∼13:00 UT and $-77°\Lambda$, rapidly expanded equatorward until about ∼13:20 UT and $-69°\Lambda$. This feature then gradually migrated further equatorward and lost its identity, though perhaps re-emerging as the start of a stronger feature at ∼13:40 UT and $-68°\Lambda$. Yet another power enhancement, perhaps commencing as early as 13:50 UT and $-72°\Lambda$, also merged into the main feature at ∼14:25 UT and $-64°\Lambda$. Overall, the behaviour of the power enhancements was complex, and the reader will recognise other features expanding equatorward throughout the study interval.

Figure 3b shows a sequence of equatorward propagating flow bursts to speeds ∼500 m/s, primarily toward the radar, but sometimes weakly away from the radar. For example, major equatorward flow burst (red) commenced at about 12:32 UT and $-74°\Lambda$, 13:00 UT and $-76°\Lambda$, 13:06 UT and $-78°\Lambda$ (the largest patch of red), 13:23 UT and $-74°\Lambda$, and 14:35 UT and $-74°\Lambda$. Most of the major flow bursts had a lifetime of ∼8 min, but were bifurcated, and numerous lesser flow bursts (red) also occurred before and after. Taking the time differences between successive flow bursts (including lesser events) and then averaging, we obtain a quasi-period of 10.5 min, but the eye tends to ignore both longer periods and fine details.

Figure 4 is a power spectrum of the LOS Doppler velocities recorded at the range of 1800 km shown in Fig. 3b. Ideally, the 2-D spectrum of Fig. 3b should be calculated, because the frequency and amplitude of the spectral peaks changes with range, but the results shown in Fig. 4 are reasonably representative. Significant power in all of the spectra begins for periods >8 min, and in this case a dominant peak occurs at 24 min. The relationship between the periods present in nightside flow bursts and magnetospheric reconnection needs to be investigated.

There was a tendency for the equatorward propagating power enhancements to grow in intensity at the times when strong flow bursts occurred. For example, during 13:00–13:30 UT, when B_z briefly swung northward, there were at least three major flow bursts and a comparable number of power enhancements, but the latter seemed to survive beyond the flow bursts. For example, the power enhancement commencing at ∼13:00 UT and $-77°\Lambda$ expanded equatorward at a fairly constant rate until about ∼13:20 UT and $-70°\Lambda$. This implies a patch of decameter-scale irregularities expanded equatorward with a velocity of ∼650 m/s, comparable to the maximum LOS velocity in the concurrent flow burst. In general, the equatorward expansion of the power enhancements tended to decrease with latitude in a similar way to the LOS velocities.

It was tempting to associate every power enhancement with an individual flow burst, but clearly there was a poor correlation between the two parameters across the entire record. This complex behaviour can be reconciled with the gradient-drift instability, if it was responsible for the iono-

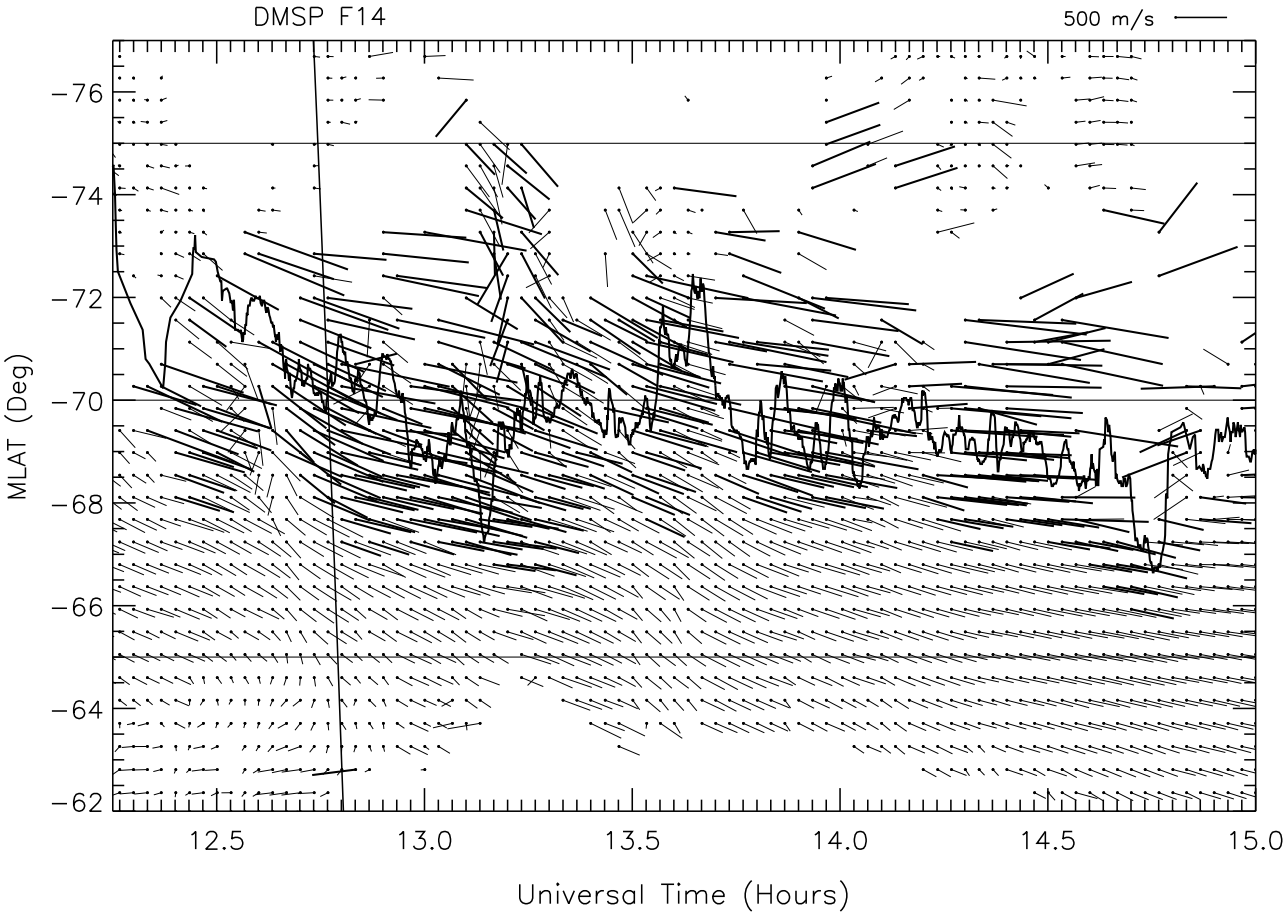

Fig. 5. Two-dimensional flow vectors estimated along TIGER beam 4 using the beam-swinging technique at 2-min time resolution during 12:15 to 15:00 UT, 10 December 1999. The solid dots correspond to the time and latitude of the velocity estimate, and the flows were in the direction of the lines leaving the dots. Flows directed toward the right were eastward, and toward the bottom, equatorward. The scale for an eastward flow of 500 m/s is shown at top right. Flows with magnitudes >400 m/s were drawn in bold to emphasize the flow bursts commencing on open field lines. The same SWB shown in Fig. 3 has been superimposed in bold. The diagonal line starting at 12:45 UT represents the transit of the DMSP F14 satellite (c.f., Fig. 2).

spheric irregularity production (and thus, power enhancements). The growth rate of gradient-drift waves is largest when the term $\boldsymbol{v} \cdot \delta n_e/n_e \boldsymbol{i}$ is large and positive, where $v = E/B$ is the ion drift speed (Kelley, 1989). Synthesis of the power enhancements shown in Fig. 3a would require detailed knowledge of the production, loss, and transport of ionospheric plasma, as well as the two-dimensional convection velocities throughout the radar FOV. The latter might be obtained using beam-swinging (Fig. 5), or more reliably, using a second radar with overlapping FOV.

We speculate that intense irregularity production occurred at the trailing edges of electron density patches where the plasma drifted in the same direction as the plasma density gradient. While still on open field lines, the electron density patches were probably accelerated equatorward by the nightside flow bursts, initiating intense irregularity production in the process. The electron density patches traversed the OCB and entered the auroral oval where their identity was either lost or greatly enhanced, depending on coincidence with fluctuating particle precipitation. The electron density patches eventually became F-region boundary blobs, well-known to form in the poleward wall of the main ionospheric trough (e.g. see Jones et al., 1997). Indeed, the largest SNRs (>36 dB) observed may have been caused by total reflections from (or within) an irregular, poleward wall of the main trough.

Although there is no direct corroborating evidence for the preceding interpretation, it is plausible because (1) intense decametre-scale irregularity production probably occurs in the presence of sharp horizontal gradients in electron density (i.e. the ionosphere was very patchy), (2) the power enhancements were first detected on open field lines at the poleward limit of scatter (i.e. polar cap patches), and (3) their equatorward motion slowed in accordance with the equatorward decrease in LOS Doppler velocity (i.e. the patches were mostly convecting). An alternative explanation, namely the power enhancements were controlled by curtains of precipitation expanding equatorward from the polar cap at a non-

convective velocity, does not fit all the available observations.

Rodger et al. (1994) reported simultaneous inter-hemispheric observations of polar patches in the nightside ionosphere. Their observations also suggested an association between equatorward propagating power enhancements and large LOS Doppler velocities. However, the SNR of their observations was ∼15 dB lower than ours, probably resulting in an absence of echoes outside their patch signatures, so the association was not proven. Breed et al. (2001) used a digital ionosonde to observe velocity surges at the edges of electron density patches passing above the polar cap station Casey ($-81°\Lambda$). Their results suggest that SuperDARN radars will observe irregularity patches formed by large velocities driving the gradient drift instability at the edges of electron density patches.

Simultaneous observations of the dayside ionosphere made with the Halley radar during this event (see Parkinson et al., 2002 for a description of these coordinated experiments) showed sparse scatter with large receding velocities, possibly indicative of dayside flow bursts during these moderately disturbed conditions ($B_z \sim -3$ nT). However, the continuity of the Halley radar data was not sufficient to ascertain whether the nightside flow bursts shown in Fig. 3b were synchronised with signatures of dayside reconnection. In addition, the nightside flow bursts were not synchronised with fluctuations in the IMF (Fig. 1b and c), as would be expected if the dayside DP 2 current system dominated the entire high-latitude ionosphere. By itself, this suggests the nightside flow bursts were the signature of nightside reconnection.

Figure 5 shows the two-dimensional flow vectors estimated along TIGER beam 4 using the LOS Doppler velocities measured on all radar beams and the beam-swinging technique described by Ruohoniemi et al. (1989). The technique is only accurate for reasonably laminar flows with constant velocity along magnetic L-shells (Freeman et al., 1991). An absence of flow vectors in the plot is usually an indication that echoes with good SNR were detected on an insufficient number of beams. However, sometimes it indicates that the algorithm did a reasonable job of detecting when the assumption of uniform motion along L-shells was not well satisfied.

Figure 3b shows that the flow bursts in LOS velocity were often to apparent speeds of >500 m/s, but recall they may have been partly due to changes in flow direction (Chisham et al., 2000). Figure 5 shows the decametre irregularities were nearly always drifting toward the east and equatorward. The flow bursts were up to true speeds of 1 km/s in a similar direction, but sometimes at lower speed toward the radar. The flow bursts were superimposed on a background of slower drifts poleward of $-68°\Lambda$. The flows immediately equatorward of the high speed regime (bold) decreased rapidly over $\sim 1°\Lambda$, becoming as low as 100 m/s at the equatorward limit of backscatter ($\sim -62°\Lambda$). However, they were essentially a more uniform continuation of the erratic flows observed at higher latitudes.

An exception to the generally eastward and equatorward flows occurred at latitudes equatorward of $-65°\Lambda$ before 12:45 UT, when beam 4 probably passed through the Harang discontinuity. Referring back to Fig. 3a, the SNR patches also intensified beyond the signature of the Harang discontinuity. This implies that the plasma circulating within the dawn convection cell had a history more conducive to the formation of decametre-scale irregularities than the plasma circulating within the dusk convection cell. Tsunoda (1988) argued that the difference between the ion and neutral velocities is consistently greater in the post-midnight sector, and, therefore, stronger irregularity growth should occur there.

Figure 3c reveals a persistent, sharp SWB between an $\sim 10°\Lambda$ wide poleward region of scatter with spectral widths primarily >200 m/s (red and green), and an $\sim 5°\Lambda$ wide equatorward region with spectral widths <50 m/s (black and blue). The boundary had a width comparable to two range pixels (90 km), or less than $1°\Lambda$. It was located near $-69°\Lambda$, but fluctuated ∼200 km in range on a time scale of ∼10 min (though other time scales were present; cf., Fig. 4). The SWB was automatically identified by choosing the most equatorward range cell which had a spectral width <200 m/s, while the next furthest range cell had a spectral width ≥200 m/s, and the subsequent three range cells had a spectral width ≥100 m/s. This scheme prevented multiple, perhaps spurious identifications of the SWB on the basis of large, isolated spectral widths. The corresponding SWB is superimposed in bold in all panels of Fig. 3 and Fig. 5.

Fluctuations in the location of the SWB resembled the equatorward limit of LOS Doppler velocity >300 m/s shown in Fig. 3b, but clearly there was no one-to-one correspondence. Figure 5 shows that the flow bursts (bold) usually commenced on open field lines, and then crossed over the SWB. The larger LOS Doppler velocities associated with the flow bursts sometimes penetrated to the equatorward edge of scatter with low spectral width (e.g. at 13:11 UT), but there was usually a rapid decrease in velocity (∼400 to 100 m/s) within several degrees equatorward of the SWB.

Figure 3c also shows that the nightside SWB was located at $\sim -74°\Lambda$ at 12:25 UT, and towards the end of the record it reached its equatorward limit of $\sim -67°\Lambda$ at 14:45 UT. Near the start of the record the SWB may have been bifurcated, simultaneously located at $-72°\Lambda$ and $-74°\Lambda$ at 12:25 UT. However, for most of the study interval there was essentially one SWB with numerous fluctuations in location and time, but little net motion toward the equator.

There was a complex relationship between rapid expansions and contractions of the SWB, and the individual flow bursts shown in Figs. 3b and 5. The spatial coverage of the observations was not sufficient to determine whether individual flow bursts were associated with dayside or nightside reconnection. However, the rapid poleward contractions of the SWB associated with some of them (e.g. 13:09 and 13:33 UT) resembled the predicted response of the midnight OCB to nightside reconnection, as depicted in Fig. 7 of Cowley and Lockwood (1992).

Overall, the behaviour of the SWB was consistent with a balance between the effects of dayside and nightside reconnection, causing successive expansions and contractions of the polar cap boundary, respectively. Hence, the behaviour

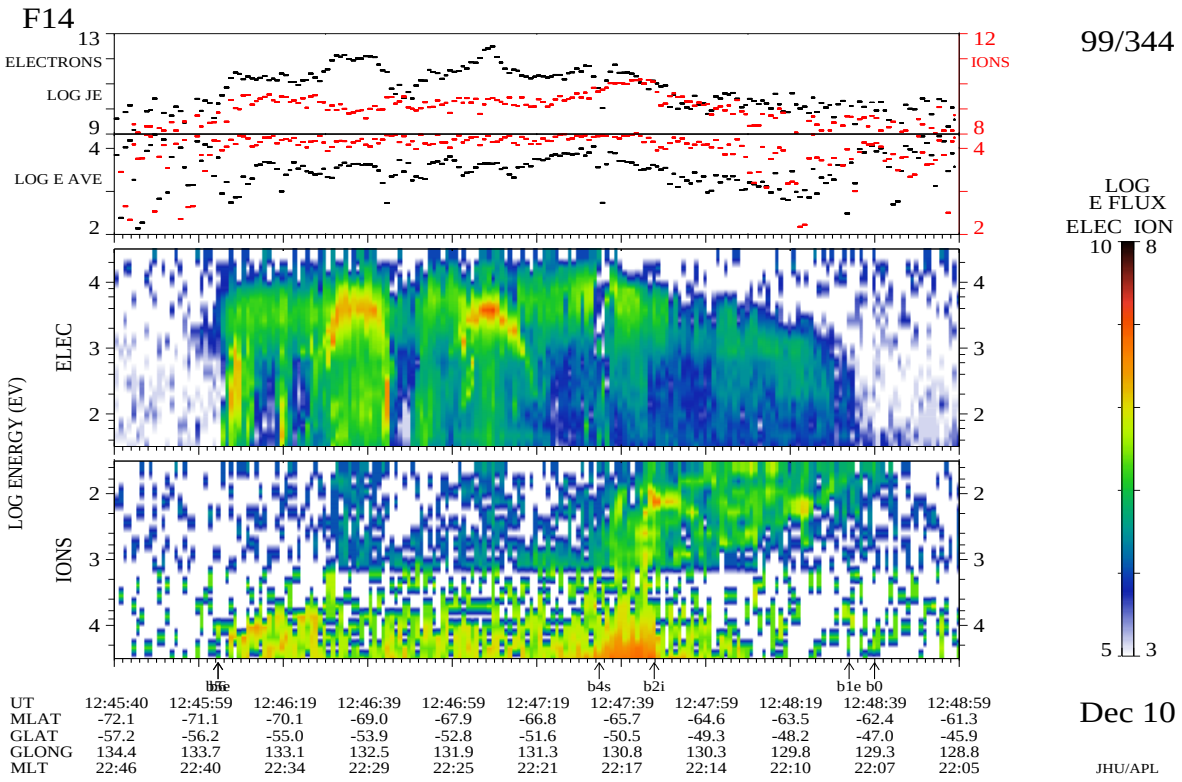

Fig. 6. Spectrograms calculated from 1 s resolution measurements of precipitating ions and electrons made with the SS J/4 detector on board the DMSP F14 spacecraft during 12:45:40 to 12:48:59 UT on 10 December 1999. The top and second panels show the base-10 logarithms of the integral energy flux (eV $cm^{-2}s^{-1}ster^{-1}$), and average energy (eV) carried by the ions (red) and electrons (black), respectively. The bottom two panels show the spectra of differential energy flux (eV $cm^{-2}s^{-1}ster^{-1}eV^{-1}$) for the precipitating ions and electrons, again on logarithmic scales. Note that ion energy increases downwards. The abscissa is annotated with universal time (UT), magnetic latitude (MLAT), geographic latitude (GLAT), geographic longitude (GLONG), and the magnetic local time (MLT). The nominal OCB corresponds to the boundary b5e (near 12:45:59 UT), the transition between discrete and diffuse aurora to the boundary b4s (near 12:47:39 UT), and the plasmapause in proximity to the boundaries b1e and b0 (near 12:48:39 UT).

of the SWB was not consistent with a sustained adiaroic expansions of the polar cap boundary (i.e. no flow across it). However, eventually the dayside driver dominated, and an equatorward expansion of the entire region of backscatter reminiscent of the HF growth phase signature of a magnetospheric substorm (Lewis et al., 1998) ensued toward the end of the study interval (cf. Fig. 1e). Although many of the flow bursts were probably driven by nightside reconnection, it seems likely that eventually dayside reconnection caused a net equatorward expansion of the polar cap boundary just prior to a minor substorm.

The scatter with low spectral widths was also similar to the population of echoes described as dusk scatter associated with the main ionospheric trough (Ruohoniemi et al., 1988). Dusk scatter has a mode spectral width of 12 m/s, close to the mode value of our observations. Other related phenomena include slow long-lived E-region plasma structures (SLERPS) (Jayachandran et al., 2000), and echo regions corresponding to the subvisual equatorward edge of the diffuse luminosity belt (SEEL) (Uspensky et al., 2001). We speculate these phenomena represent the same underlying phenomena observed in different ways because each radar has a different location relative to the backscattering irregularities. The underlying phenomenon responsible for the ionospheric echoes with low spectral width is probably just the $\boldsymbol{E} \times \boldsymbol{B}/B^2$ motion of secondary gradient drift waves within the E- and F-regions, with little or no perturbation by Pc 1–2 hydrodynamic wave activity.

Note that most of the SuperDARN radars are located further poleward than TIGER, and they cannot observe the full latitudinal extent of the auroral oval beyond the dusk sector. Even then, the auroral oval echoes may only be observed in a narrow range window relatively close to the radar, depending on where the radio waves are refracted by the ionosphere to achieve normal incidence on the field lines. The hypothesis that auroral and subauroral scatter is more completely observed using TIGER because of its more equatorward location needs testing using ray tracing through realistic ionospheres.

Figure 6 shows spectrograms calculated from precipitating ions and electrons measured on board the DMSP F14 satellite during the transit shown in Fig. 2. The labels b0,

b1e, b2i, etc. are nightside auroral oval boundaries automatically identified using the logical criteria (not a neural net) outlined by Newell et al. (1996). The boundaries b0, b1e, and b1i represent the first point at which precipitation above the noise level was identified, and the "zero energy" electron and ion boundaries, respectively. They all nearly coincide, having values of $-62.4°$, $-62.7°$, and $-62.4°\Lambda$, respectively. Hence, they can be interpreted as indicating the approximate location of the plasmapause (Nishida, 1966; Horwitz et al., 1986; and Newell et al., 1996).

As Fig. 3c implies, the approximate location of the aforementioned boundaries ($-62.4°\Lambda$) was coincident with the equatorward limit of the scatter with very low spectral widths traversed by the satellite track at 12:48 UT. This implies the equatorward limit of the scatter mapped to the plasmapause, and probably also the main ionospheric trough. However, we speculate that $-62.4°\Lambda$ was actually the location of the poleward wall of the trough, because this structure is known to coincide with the equatorward limit of the diffuse auroral oval. Moreover, the power enhancements shown in Fig. 3a expanded equatorward until they reached the equatorward limit of the diffuse auroral oval, as would be expected if they were associated with F-region boundary blobs. The possibility that short-term fluctuations in the scatter boundary represents fluctuations in the location of the trough wall needs further investigation.

The boundary b2e=$-66.0°\Lambda$ (no label) is the point where the electron average energy is neither increasing nor decreasing, and is one interpretation of the start of the CPS (Newell et al., 1996). However, the inner edge of the CPS often extends equatorward to the plasmapause (Kivelson and Russell, 1995). The boundaries b3a=$-67.0°\Lambda$ and b3b=$-68.9°\Lambda$ were the equatorward and poleward limits of electron acceleration events, respectively. There were few monoenergetic spectra characteristic of these events during this moderately disturbed interval. Of greater relevance to this study, the boundary b4s=$-66.0°\Lambda$ is the boundary between discrete and diffuse precipitation, and the boundaries b5e=$-70.9°\Lambda$ and b5i=$-70.8°\Lambda$ are the poleward boundaries of the auroral oval (i.e. the OCB), the latter determined by abrupt drops in electron and ion precipitation, respectively. The label b5e is superimposed on another label in Fig. 6.

At the corresponding instants along the satellite track shown in Fig. 3, the region with flow bursts >300 m/s was confined to latitudes ~ -70.4 to $-75.0°\Lambda$ (part b), and the sharp SWB was located close to $\sim -70.4°\Lambda$, but changing rapidly in time (part c). Given that the DMSP satellite observed the diffuse and discrete auroral ovals between $-62.4°\Lambda$ and $-70.9°\Lambda$, we associate the small spectral width scatter (blue and black) with the discrete and diffuse auroral ovals (i.e. closed field lines), and the large spectral width scatter with the polar cap ionosphere (i.e. open field lines). Within the accuracy of the magnetic mappings, the nightside SWB was a proxy for the OCB at this time, and the equatorward edge of the scatter with low spectral width was a proxy for the poleward wall of the main ionospheric trough.

Strictly speaking, to identify the SWB with the OCB on a reproducible basis, we should find agreement with many coincident spacecraft observations throughout numerous study intervals, but the single identification made here was reliable, and the subsequent behaviour of the SWB was entirely consistent with the expected behaviour of the OCB (cf., Fig. 7 of Cowley and Lockwood, 1992). Moreover, we have found similar associations in case study data recorded on other nights. However, note that Lester et al. (2001) concluded that the SWB can be used as a proxy for the OCB, but only with extreme caution.

Figure 2 shows that the satellite track passed through TIGER beam 4, range cell 48 ($-77.0°\Lambda$) near 12:44:00 UT, and through beam 0, range cell 39 ($-72.4°\Lambda$) near 12:45:35 UT. Hence, the satellite track was actually slightly to the west of beam 0 when it traversed the discrete and diffuse auroral ovals and the nightside OCB ($-70.5°\Lambda$). The concurrent 96 s resolution full-scan measurements (not shown) revealed longitudinal structure in the SWB, but the latter was essentially aligned in the magnetic zonal direction. Therefore, it seems reasonable to extrapolate the DMSP OCB to beam 4, located $\sim 15°$ to the east. It was important to use the beam 4 high-time resolution (6 s) measurements, because the radar features were very dynamic, changing by $\sim 1°\Lambda$ during the few minutes before or after the satellite pass. Allowing for small errors due to the longitudinal separation of the DMSP track and beam 4, we consider the TIGER boundary identifications to be reliable.

Some evidence corroborating the DMSP OCB identification was found using NOAA-15 satellite measurements of the pitch-angle distribution of protons and electrons with energy >30 keV. When the pitch-angle distributions are anisotropic, the particles are probably trapped radiation belt particles mirroring on closed field lines. When the pitch-angle distributions become isotropic and the intensity (particles $cm^{-2}s^{-1}ster^{-1}$) becomes relatively low, the particles are probably on open field lines. The OCB should also agree with the poleward edge of the auroral oval identified by a reduction in the integral energy flux (ergs $cm^{-2}s^{-1}$) of protons and electrons with energies 50 eV to 20 keV, as measured independently on board the same spacecraft.

Applying the previous criteria to the most relevant pass of a NOAA satellite, the OCB was identified at 13:03:45 UT (20:31 MLT), and $-72.3°\Lambda$. The nightside SWB identified in the TIGER data at 13:04 UT (23:30 MLT) was located at $-70°\Lambda$, or 2.3° equatorward of the NOAA-15 boundary. However, model auroral oval boundaries for $K_p=2$ ($AL=-86$) (Starkov, 1994a, b) place the poleward edge of the auroral oval at $-72.6°\Lambda$ at 20:31 MLT, and $-70.7°\Lambda$ at 23:30 MLT. By allowing for a 1.9° diurnal variation of the auroral oval location, and the inevitable longitudinal structure, this implies that the NOAA-15 OCB and TIGER SWB were in reasonable agreement. Certainly it would be a gross error to associate the NOAA-15 boundary with any other major feature in the TIGER data, such as the equatorward limit of scatter with low spectral width or the poleward limit of scatter with high spectral width.

The flow bursts shown in Figs. 3b and 5 occurred primarily in the pre-midnight sector near the exit of the polar cap flow, with the fastest, most erratic flows confined between latitudes $-67°$ and $-77°\Lambda$. The coincident DMSP and NOAA measurements imply that the flow bursts must have commenced on open field lines mapping to the southern tail lobe, and converging upon a reconnection site in the neutral sheet. The midnight OCB sometimes contracted poleward in the process of the corresponding open field lines traversing the OCB and subsuming into the equatorward region of slowly moving closed field lines. In a sense, the closed field lines earthward of the OCB formed a "barrier" to the fast magnetospheric convection at higher latitudes. Figure 5 shows that the motion of closed field lines (equatorward of $\sim -68°\Lambda$), ejected from the reconnection site, was much slower and more laminar than the motion of open field lines. Note that patches of enhanced SNR (Fig. 3a) were probably drifting at the $\boldsymbol{E} \times \boldsymbol{B}/B^2$ velocity, and they migrated across the OCB; hence, by definition, they imply that nightside reconnection must have taken place.

There was no distinct signature of an ionospheric boundary separating the discrete and diffuse auroral ovals in the TIGER observations during the study interval. Perhaps the nightside BPS/CPS boundary signature (as observed by Dudeney et al., 1998) is formed when discrete auroral activity and nightside reconnection processes are more vigorous, in which case a more gradual SWB might be observed. The different qualitative character and interpretation of nightside SWB observations needs to be reconciled by analysing observations made under a broad range of geophysical conditions.

It is generally believed that near-range ($\leq$600 km) ionospheric scatter observed by SuperDARN radars emanates from E-region irregularities, whereas the far-range scatter (e.g. Fig. 3) emanates from F-region irregularities. However, when the energy of precipitating electrons is sufficiently large ($>$1 keV), the true height profile of ionospheric electron density can peak in the E-region ($<$150 km) due to the additional plasma created via collisional excitation. Hence, it seems reasonable to wonder whether the scatter with large spectral widths (red; Fig. 3c) was associated with F-region irregularities, and the auroral scatter with small spectral widths (blue and black) was associated with E-region irregularities, possibly generated by an entirely different plasma instability.

However, we believe that the backscatter with low spectral widths ($<$50 m/s) emanated from the F-region, because the elevation angle data recorded with the TIGER subarray did not show a distinct transition across the SWB, as might be expected if two separate height regimes were involved. Even if the backscatter with low spectral widths did emanate from the E-region, this is a mute point, because the LOS Doppler velocities for both kinds of scatter were fairly consistent with the results of F-region convection models showing the $\boldsymbol{E} \times \boldsymbol{B}/B^2$ drift of plasma. Finally, Jayachandran et al. (2000) argued that closely related E-region phenomena, SLERPS, drift at the F-region convection velocity, because their LOS Doppler velocities are less than the ion acoustic speed. The latter limits the excitation of type I two-stream instabilities (Farley, 1963; Buneman, 1963).

Experience with analysing TEC measurements and ionograms recorded under a broad range of geophysical conditions (not shown) helped to validate the DMSP-inferred locations of the auroral oval and main ionospheric trough relative to the TIGER backscatter. Horvath and Essex (2000, 2001) describe the dual frequency group- and phase-path technique used to calculate TEC, and the subsequent identification of the trough. Vertical TEC values were calculated using the Global Positioning System (GPS) satellites visible with ground-based receivers located at TBL ($-46°\Lambda$), HOB ($-54°\Lambda$), and MQI ($-65°\Lambda$). The trough was best observed when both the middle of the trough and a GPS satellite passed directly overhead. For example, a deep trough was often identified above HOB under very disturbed conditions.

The location of the main trough was not directly identified in TEC measurements made during 12:00 to 15:00 UT on 10 December, partly because the oblique paths to the GPS satellites traversed large, fluctuating electron densities in the auroral zone before intercepting the trough located further equatorward. During 12:00 to 15:00 UT, there was a large enhancement in TEC ($> 80 \times 10^{16}$ electrons m^{-3}), indicating auroral precipitation in the ionosphere above MQI ($-65°\Lambda$). This is consistent with the DMSP measurements made further to the west, which identified the boundary between discrete and diffuse auroral ovals at $-66°\Lambda$. When judged in the context of observations made on other days, the TEC observations imply where the trough should have been.

Similarly, routine ionograms recorded by the ionosondes located at HOB and MQI did not directly identify the trough during the evening of 10 December. However, very low values of *f*oF2 ($<$2 MHz) were recorded at HOB on the same days when a TEC trough was detected. The ionograms recorded at MQI on 10 December showed the frequent disappearance of traces caused by enhanced D-region absorption associated with energetic particle precipitation. Specifically, during 12:00 to 15:00 UT auroral E traces were observed (i.e. the diffuse auroral oval), but from 15:15 UT onwards, the auroral traces also disappeared from the ionograms, probably due to D-region absorption associated with very energetic aurora passing overhead.

In summary, experience with TEC and ionosonde data recorded on a variety of days with different levels of geomagnetic activity are entirely consistent with an auroral oval located above $-65°\Lambda$ and the trough equatorward but nearby at $\sim -62°\Lambda$ on 10 December.

3 Conclusions and future work

The IMF B_z component was primarily southward at about -3 nT, and the MQI magnetometer data indicated moderate growth phase conditions during 12:00 to 15:00 UT on 10 December 1999. This was an unusually long period for B_z to have been southward and no substorm to have been triggered, implying a sustained balance between the effects

of dayside and nightside reconnection. The TIGER HF backscatter radar observed a persistent, sharp latitudinal decrease (∼90 km) in spectral width (the SWB) located near −69° Λ and magnetic midnight. There was also a reasonably rapid decline in the LOS Doppler velocity across the boundary. The scatter poleward of the SWB was characterized by high spectral widths (>200 m/s) and the start of bursty flows with speeds up to 1 km/s toward the east and equatorward, but sometimes with slower speeds in a more equatorward direction. The flow bursts expanded equatorward across the OCB and were probably driven by nightside reconnection. The scatter equatorward of the SWB was characterized by very low spectral widths (<50 m/s) and slower, more laminar eastward and equatorward flows (100–400 m/s).

The ionospheric track of the DMSP F14 satellite was coincident with TIGER observations made at 12:45 UT, enabling the location of the discrete and diffuse auroral ovals to be fixed with respect to the scatter with low spectral width. The results imply that the SWB must have been a proxy for the OCB at that time. Moreover, the usually persistent scatter with large spectral widths (>200 m/s) must have been associated with irregularities forming on the open (but soon to be reconnected) field lines, threading the polar cap to the southern tail lobe. The beam-swinging analysis showed the flow bursts extended for ∼2° across the OCB, but decayed rapidly within the regime of the closed field lines mapping to the auroral ionosphere. The usually transient scatter with small spectral widths (<50 m/s) was associated with irregularities residing on the slower moving closed field lines, threading the discrete and diffuse auroral oval to the PSBL (if it existed), but almost certainly to the CPS.

There is a kind of symmetry between the dynamics associated with the dayside and nightside SWBs observed using SuperDARN radars. In the dayside ionosphere, the equatorward limit of the scatter with large spectral widths (>200 m/s) is a proxy for the OCB. Magnetic field lines immediately equatorward of the SWB probably thread to a merging site in the outer LLBL (closed field lines), and magnetic field lines immediately poleward of the SWB must have entered the polar cap (open field lines). In the nightside ionosphere, the equatorward limit of the scatter with large spectral widths (>200 m/s) is also a proxy for the OCB. However, magnetic field lines immediately equatorward of the SWB probably thread to a merging site in the PSBL or outer CPS (closed field lines), whereas magnetic field lines immediately poleward of the SWB are just about to leave the polar cap (open field lines).

Concerning what causes the enhanced spectral widths, Schiffler et al. (1997) identified double-peaked Doppler spectra observed by SuperDARN radars in proximity to the ionospheric footprint of the outer low-latitude boundary layer. They suggested that small-scale convection vortices with a scale size less than the radar resolution (∼100×45 km at 1500 km) caused these spectra. Huber and Sofko (2000) established an upper limit of ∼26 km for the scale size and ∼4 s for the lifetime of these vortices. The FITACF algorithm will assign large spectral widths to echoes producing multi-component Doppler spectra. The enhanced spectral widths observed in the nightside polar cap ionosphere, as shown in Fig. 3c, may have been caused by small-scale vortices that are primarily confined to open magnetic field lines.

Similarly, the enhanced spectral widths may also have been driven by a population of Pc 1–2 hydrodynamic waves that only occur on open field lines (hence, their source may be in the magnetosheath, foreshock, or solar wind). This is the same hypothesis used to model successfully the enhanced spectral widths observed in the dayside cusp region (André et al., 1999, 2000a, 2000b). André and Freeman (Private Communication, 2001) have also modelled the gradual nightside SWB reported by Dudeney et al. (1998), showing that it can be explained by the coincident Pc 1–2 electric field fluctuations recorded on board the Polar spacecraft. Other TIGER observations we have examined also support this hypothesis, but further analyses are required to establish whether the explanation can be generalised to all nightside SWB observations.

There was no evidence for different scatter regions corresponding to the PSBL/BPS and CPS. It should be possible to clarify the magnetosphere-to-ionosphere mappings of these different regions using future CLUSTER and GEOTAIL spacecraft traverses of the magnetotail when their orbits map to within the TIGER FOV. It would also be interesting to use multi-radar full-scan data to investigate the longitudinal structure in the SWB, thereby defining the detailed shape of the SWB, and the way it expands and contracts across the merging gap. Bifurcated SWBs might imply the existence of "islands" of open (closed) magnetic flux, detached equatorward (poleward) from the true polar cap (auroral oval). The same data might also be used to investigate substorm signatures in the nightside ionosphere, another topic ideally suited to TIGER observations due to its more equatorward latitude.

Patches of enhanced backscatter power were observed moving equatorward and eastward out of the polar cap ionosphere, especially after beam 4 measurements detected a signature of the Harang discontinuity near 12:45 UT. There was a vague association between the power enhancements and flow bursts, as would be expected if the gradient drift instability were operative. The patches either lost their identity or were reinforced (or new ones appeared) as they drifted equatorward through the auroral oval. Their equatorward motion declined toward zero, becoming more zonal as they moved toward the equatorward limit of backscatter. We speculate that the power enhancements were caused by intense ionospheric irregularities forming in association with electron density patches drifting out of the polar cap, and eventually becoming boundary blobs in the poleward wall of the trough.

The combined interpretation of the DMSP, NOAA-15, TEC, and ionosonde data suggested the equatorward limit of the region with low spectral width probably aligned with the poleward wall of the main ionospheric trough, thus, helping to infer the likely location of the plasmapause. It is likely that scatter overlapping the plasmapause footprint and extending

into the true mid-latitude ionosphere is often observed by TIGER at MLTs well before and after midnight.

The observations presented in this paper were of exceptional quality, partly because a very sharp spectral width boundary (SWB) persisted for over 3 hours under moderately disturbed conditions (ΣK_p=18$^+$). However, preliminary analyses of observations made on the following, less disturbed night of 11 December 1999 (ΣK_p=13$^+$), and other more disturbed nights, also support the results of this study. On the other hand, ionospheric dynamics can be far more complex, and the corresponding magnetospheric boundaries more difficult to identify, during substorms. We recommend the detailed analysis of many more coincident SuperDARN, satellite, and ionosonde observations made under a broad range of geophysical conditions. Only then can generalisations be made about the universal nature of the nightside SWB.

Acknowledgements. This work was supported by the Australian Research Council, the Australian Antarctic Science Advisory Committee, the UK's Natural Environment Research Council, Australian Antarctic Division, DSTO Salisbury, the Ian Potter Foundation, RLM Systems Pty. Ltd, and the State Government of Tasmania. We thank R. Lepping and K. Ogilvie of Goddard Space Flight Center for making Wind magnetic field and solar wind data freely available over the internet. We thank Simon Wing of the John Hopkins University Applied Physics Laboratory for making DMSP SS J/4 dynamic spectra available over the internet, and checking the magnetic coordinate transformations. The distribution of the DMSP ion flow data examined in this study were supported by NASA under grant NAG5–9297. We also thank David Evans of the Space Environment Centre and National Oceanic and Atmospheric Administration for providing NOAA-15 radiation belt data. Finally, we thank the numerous people who contributed to the construction, development, and maintenance of TIGER.

Topical Editor M. Lester thanks W. Bristow and another referee for their help in evaluating this paper.

References

Anderson, P. C., McCrea, I. W., Strickland, D. J., Blake, J. B., and Looper, M. D.: Coordinated EISCAT/DMSP measurements of electron density and energetic electron precipitation, J. Geophys. Res., 102, 7421–7430, 1997.

André, R., Pinnock, M., and Rodger, A. S.: On the SuperDARN autocorrelation function observed in the ionospheric cusp, Geophys. Res. Lett., 26, 3353–3356, 1999.

André, R., Pinnock, M., and Rodger, A. S.: Identification of the low-altitude cusp by Super Dual Auroral Radar Network radars: A physical explanation for the empirically derived signature, J. Geophys. Res., 105, 27081–27093, 2000a.

André, R., Pinnock, M., Villain, J.-P., and Hanuise, C.: On the factors conditioning the Doppler spectral width determined from SuperDARN HF radars, Int. J. Geomag. Aeronomy, 2, 77–86, 2000b.

André, R., Pinnock, M., Villain, J.-P., and Hanuise, C.: Influence of magnetospheric processes on winter HF radar spectra characteristics, Ann. Geophysicae, In Press, 2002.

Baker, K. B. and Wing, S.: A new magnetic coordinate system for conjugate studies of high-latitudes, J. Geophys. Res., 94, 9139–9143, 1989.

Baker, K. B., Dudeney, J. R., Greenwald, R. A., et al.: HF radar signatures of the cusp and low-latitude boundary layer, J. Geophys. Res., 100, 7671–7695, 1995.

Blanchard, G. T., Lyons, L. R., Samson, J. C., and Rich, F. J.: Locating the polar cap boundary from observations of 6300Å auroral emission, J. Geophys. Res., 100, 7855–7862, 1995.

Blanchard, G. T., Lyons, L. R., and Samson, J. C.: Accuracy of using 6300Å auroral emission to identify the magnetic separatrix on the nightside of Earth, J. Geophys. Res., 102, 9697–9703, 1997.

Breed, A. M., Maddern, T. M., Dyson, P. L., and Morris, R. J.: Dynamics of the polar cap ionosphere, Part 2. Case studies of polar patches above Casey, Antarctica, ANARE Reports, 146, 189–208, 2001.

Buneman, O.: Excitation of field-aligned sound waves by electron streams, Phys. Rev. Lett., 10, 285, 1963.

Carpenter, D. L. and Park, C. G.: On what ionospheric workers should know about the plasmapause-plasmasphere, Rev. of Geophys. and Space Phys., 11, 133–154, 1973.

Chisham, G., Pinnock, M., and Rodger, A. S.: Poleward-moving HF radar flow bursts in the cusp: Transient changes in flow speed or direction? Geophys. Res. Lett., 27, 919–922, 2000.

Cowley, S. W. H. and Lockwood, M.: Excitation and decay of solar wind-driven flows in the magnetosphere-ionosphere system, Ann. Geophysicae, 10, 103–115, 1992.

Dudeney, J. R. and Rodger, A. S.: Ionospheric signature of plasma sheet thinning prior to a substorm, Planet. Space. Sci., 36, 1285–1293, 1988.

Dudeney, J. R., Rodger, A. S., M. P. Freeman, Pickett, J., Scudder, J., Sofko, G., and Lester, M.: The nightside ionospheric response to IMF B_y changes, Geophys. Res. Lett., 25, 2601–2604, 1998.

Dyson, P. L. and Devlin, J. C.: The Tasman International Geospace Environment Radar, The Physicist (The Australian Institute of Physics), 37, 48–53, March/April, 2000.

Evans, L. C. and Stone, E. C.: Electron polar cap and the boundary of open geomagnetic field lines, J. Geophys. Res., 77, 5580, 1972.

Farley, D. T.: A plasma instability resulting in field-aligned irregularities in the ionosphere, J. Geophys. Res., 68, 6083, 1963.

Freeman, M. P., Ruohoniemi, J. M., and Greenwald, R. A.: The determination of time-stationary 2-D convection patterns with single station radars, J. Geophys. Res., 96, 15 735–15 749, 1991.

Greenwald, R. A., Baker, K. B., Hutchins, R. A., and Hanuise, C.: An HF phased-array radar for studying small-scale structure in the high-latitude ionosphere, Radio Sci., 20, 63–79, 1985.

Greenwald, R. A., Baker, K. B., Dudeney, J. R., et al.: DARN / SuperDARN: A global view of the dynamics of high-latitude convection, Space Sci. Rev., 71, 761–796, 1995.

Henderson, M. G., Reeves, G. D.: Belian, R. D., and Murphree, J. S.: Observations of magnetospheric substorms occurring with no apparent solar wind/IMF trigger, J. Geophys. Res., 101, 10 773–10 791, 1996.

Horvath, I. and Essex, E. A.: Using observations from the GPS and TOPEX satellites to investigate night-time TEC enhancements at mid-latitudes in the southern hemisphere during a low sunspot number period, J. Atmos. Solar-Terr. Phys., 62, 371–391, 2000.

Horvath, I. and Essex, E. A.: GPS and TOPEX mid-latitude trough observations in the southern hemisphere at low sunspot numbers, ANARE Reports, 146, 307–319, 2001.

Horwitz, J. L., Menteer, S., Turnley, J., et al.: Plasma boundaries in the inner magnetosphere, J. Geophys. Res., 91, 8861–8882, 1986.

Huber, M. and Sofko, G. J.: Small-scale vortices in the high-latitude F region, J. Geophys. Res., 105, 20 885–20 897, 2000.

Jayachandran, P. T., St.-Maurice, J.-P., MacDougall, J. W., and Moorcroft, D. R.: HF Detection of slow long-lived E region plasma structures, J. Geophys. Res., 105, 2425–2442, 2000.

Jones, D. G., Walker, I. K., and Kersley, L.: Structure of the poleward wall of the trough and the inclination of the geomagnetic field above the EISCAT radar, Ann. Geophysicae, 15, 740–746, 1997.

Kelley, M. C.: The Earth's ionosphere – Plasma physics and electrodynamics, Academic Press, San Diego, California, 1989.

Kivelson, M. G. and Russell, C. T. (Eds): Introduction to space physics, Cambridge Univ. Press, Cambridge, U.K., 1995.

Lepping, R. P., Acuna, M. H., Burlaga, et al.: The Wind magnetic field investigation, Space Sci. Rev., 71, 207–229, 1995.

Lester, M., Milan, S. E., Besser, V., and Smith, R.: A case study of HF radar spectra and 630.0 nm auroral emission in the pre-midnight sector, Ann. Geophysicae, 19, 327–339, 2001.

Lewis, R. V., Freeman, M. P., Rodger, A. S., Reeves, G. D., and Milling, D. K.: The electric field response to the growth phase and expansion phase onset of a small isolated substorm, Ann. Geophysicae, 15, 289–299, 1997.

Lewis, R. V., Freeman, M. P., and Reeves, G. D.: The relationship of HF radar backscatter to the accumulation of open magnetic flux prior to substorm onset, J. Geophys. Res., 103, 26 613–26 619, 1998.

Milan, S. E., Yeoman, T. K., and Lester, M.: The dayside auroral zone as a hard target for coherent HF radars, Geophys. Res. Lett., 25, 3717–3720, 1998.

Moen, J., Carlson, H. C., Milan, S. E., Shumilov, N., Lybekk, B., Sandholt, P. E., and Lester, M., On the collocation between dayside auroral activity and coherent HF radar backscatter, Ann. Geophysicae, 18, 1531–1549, 2001.

Newell, P. T., Feldstein, Y. I., Galperin, Y. I., and Meng, C.-I.: Morphology of nightside precipitation, J. Geophys. Res., 101, 10 737–10 748, 1996.

Nishida, A.: Formation of plasmapause, or magnetospheric plasma knee, by the combined action of magnetosphere convection and plasma escape from the tail, J. Geophys. Res., 71, 5669, 1966.

Ogilvie, K. W., Chornay, D. J., Fritzenreiter, R. J., et al.: SWE, A comprehensive plasma instrument for the Wind spacecraft, Space Sci. Rev., 71, 55–77, 1995.

Parkinson, M. L., Pinnock, M., and Dyson, P. L.: Variability in the response time of ghe high-latitude ionosphere to IMF and solar wind variations, Eos Trans. GU, 83(22), West. Pac. Geophys. Meet. Suppl., Abstract SP41B-09, 2002.

Pinnock, M., Rodger, A. S., Dudeney, J. R., Baker, K. B., Newell, P. T., Greenwald, R. A., and Greenspan, M. E., Observations of an enhanced convection channel in the cusp ionosphere, J. Geophys. Res., 98, 3767–3776, 1993.

Rodger, A. S. and Pinnock, M.: Movements of the mid-latitude ionospheric trough, J. Atmos. Terr. Phys., 44, 985–992, 1982.

Rodger, A. S., Brace, L. H., Hoegy, W. R., and Winningham, J. D.: The poleward edge of the mid-latitude trough-its formation, orientation and dynamics, J. Atmos. Terr. Phys., 48, 715–728, 1986.

Rodger, A. S., Pinnock, M., Dudeney, J. R., Waterman, J., de la Beaujardiere, O., and Baker, K. B.: Simultaneous two hemisphere obsrervations of the presence of polar patches in the nightside ionosphere, Ann. Geophysicae, 12, 642–648, 1994.

Ruohoniemi, J. M., Greenwald, R. A., Villain, J.-P., Baker, K. B., Newell, P. T., and Meng, C.-I.: Coherent HF radar backscatter from small-scale irregularities in the dusk sector of the subauroral ionosphere, J. Geophys. Res., 93, 12 871–12 882, 1988.

Ruohoniemi, J. M., Greenwald, R. A., Baker, K. B., Villain, J.-P., Hanuise, C., and Kelly, J, Mapping high-latitude plasma convection with coherent HF radars, J. Geophys. Res., 94, 13 463–13 477, 1989.

Schiffler, A., Sofko, G., Newell, P. T., and Greenwald, R.: Mapping the outer LLBL with SuperDARN double-peaked spectra, Geophys. Res. Lett., 24, 3149–3152, 1997.

Smith, A. J., Rodger, A. S., and Thomas, D. W. P.: Simultaneous ground-based observations of the plasmapause and F-region mid-latitude trough, J. Atmos. Terr. Phys., 49, 43–47, 1987.

Starkov, G. V.: Statistical dependencies between the magnetic activity indices, Geomag. Aeronomy, 34, 101–103, 1994a.

Starkov, G. V.: Mathematical model of the auroral boundaries, Geomag. Aeronomy, 34, 331–336, 1994b.

Tsunoda, R. T.: High-latitude F-region irregularities: a review and synthesis, Rev. Geophys., 26, 719–760, 1988.

Tsyganenko, N. A. and Stern, D. P.: Modeling the global magnetic field of the large scale Birkeland current systems, J. Geophys. Res., 101, 27 187–27 198, 1996.

Uspensky, M., Eglitis, P., Opgenoorth, H., Starkov, G., Pulkkinen, T., and Pellinen, R.: On auroral dynamics observed by HF radar: 1. Equatorward edge of the afternoon-evening diffuse luminosity belt, Ann. Geophysicae, 18, 1560–1575, 2001.

Vampola, A. L.: Access of solar electrons to closed field lines, J. Geophys. Res., 76, 36, 1971.

Web, P. and Essex, E. A.: A dynamic diffusive equilibrium model of the ion densities along plasmaspheric magnetic flux tubes, J. Atmos. Solar-Terr. Phys., 63, 1249–1260, 2001.

Winningham, J. D., Yasuhara, F., Akasofu, S.-I., and Heikkila, W. J.: The latitudinal morphology of 10-eV to 10-keV electron fluxes during magnetically quiet and disturbed times in the 21:00–03:00 MLT sector, J. Geophys. Res., 80, 3148–3171, 1975.

Woodfield, E. E., Davies, J. A., Eglitis, P., and Lester, M.: A case study of HF radar spectral width in the post-midnight magnetic local time sector and its relationship to the polar cap boundary, submitted to Ann. Geophysicae, 2002.

Yeoman, T. K., Lewis, R. V., Milan, S. E., and Watanabe, M.: An interhemispheric study of the ground magnetic and ionospheric electric fields during the substorm growth phase and expansion phase onset, J. Geophys. Res., 104, 14 867–14 877, 1999.